geosciences

MDPI

Article

Multi-Proxy Approach for Identifying Heinrich Events in Sediment Cores from Hatton Bank (NE Atlantic Ocean)

Miriam Sayago-Gil [1,*], Nieves López-González [2], David Long [3], Luis Miguel Fernández-Salas [1] and Pablo Durán-Muñoz [4]

1 Spanish Institute of Oceanography, CO. Cádiz, Puerto Pesquero, Muelle de Levante, s/n, 11006 Cádiz, Spain; luismi.fernandez@ieo.es
2 Spanish Institute of Oceanography, CO Málaga, Puerto Pesquero, s/n, 29640 Fuengirola, Málaga, Spain; nieves.lopez@ieo.es
3 Retired, Formerly: British Geological Survey, Lyell Centre, Research Ave S, Edinburgh EH14 4AP, UK; davelongmarinegeology@gmail.com
4 Spanish Institute of Oceanography, CO Vigo, Subida Radio Faro, 50, 36390 Vigo, Pontevedra, Spain; pablo.duran@ieo.es
* Correspondence: miriam.sayago@ieo.es

Received: 12 December 2019; Accepted: 23 December 2019; Published: 27 December 2019

Abstract: A series of six gravity cores has been used to reconstruct the depositional history of Hatton Bank (Rockall Plateau, NE Atlantic Ocean). The cores have been studied for magnetic susceptibility (MS), geochemical composition, grain size distribution, and a semi-quantitative foraminiferal association. Two main interbedded facies have been described: (i) calcareous ooze; and (ii) lithogenous silt. The study reveals prominent peaks from the MS signal, silt, Mg/Ca, Fe/Ca, Al/Ca, and Rare Earth Elements normalised by Continental Crust (REE/CC), which are sensitive indicators for Heinrich events (H1, H2, H3, H4, and H5) and ash layers. These peaks may relate to alternations in dominance of the calcareous and lithogenic facies. The sediment displays a high percentage of carbonate in interglacial layers but is lithogenic-dominated in glacial stages. The layers with prominent lithic-rich and foraminifera-poor sediments (established as Heinrich layers) may be related to a possible palaeoclimatic effect, where freshwater discharged during iceberg melting may have reduced the formation of North Atlantic Deep Water (NADW). In the study area, the mean sedimentation rates for the last glacial as ~4.2 cm ka^{-1} and ~1.4 cm ka^{-1} for the last ~18 ka (interglacial period) have been estimated. Besides this evidence, Fe/Ca and MS peaks may reflect the presence of basalt, either introduced through ice-rafting or transported and redistributed by bottom currents in the study area. Certain indices, including MS and Fe/Ca, are proposed as good proxies for detecting Heinrich events and ash layers in the Hatton Bank sediments and, in consequence, are parameters that can be used to infer strengthened/weakened NADW formation, according to stadials/interstadials. Moreover, we suggest that the northernmost boundary of the area with evidence of Heinrich events may be situated around 57°38′ N in the Hatton–Rockall area, at least for H4, based on the variation of the Mg/Ca and Fe/Ca curves.

Keywords: NE Atlantic; Hatton Bank; gravity cores; Heinrich events; proxies

1. Introduction

1.1. Setting

The study area is located on Hatton Bank, part of the Rockall Plateau in the northeast Atlantic Ocean, a region topographically elevated with respect to the surrounding ocean basins and isolated from terrestrial input (Figure 1). Hatton Bank is located at water depths of between 500–2800 m and is currently removed from any major supply of terrigenous sediment, being over 360 km from the closest onshore sediment source [1]. The present-day configuration of Hatton Bank is the result of a complex geological and oceanographic evolution [2]. From the mid-Miocene to the present, sediments in the NE Atlantic, in particular around the Rockall Plateau, were deposited under the influence of a persistent bottom current system. Most of the sediments are pelagic to hemipelagic deposits from sandy mud to muddy sand (mainly biogenic contourites) [3,4]. The interaction of water masses with the topography has conditioned the present distribution of the Hatton Bank sediments. The basinward slope of Hatton Bank is predominantly covered by a contourite depositional system, named Hatton Drift [5], which has been classified as a "plastered drift" [6–8] which comprises mainly mud [9]. Contourite drifts are deep-sea sediment deposits that accumulate under the influence of persistent thermohaline bottom currents [3]; these have been active at least since the Miocene [10,11] based upon DSDP holes in the study area. Bottom currents can erode, mould, transport, and redistribute sediments supplied to the slope and rise through downslope flows and vertical settling [12], as well as by alongslope transport, which is the main source of the contourite deposits [13]. Northeastward sediment transport along the Hatton Drift occurs through both suspended transport of fines in locally generated nepheloid layers and bedload transport of cohesionless sand [9]. Sediment drifts in the NE Atlantic have maintained their basic characteristics at least since the mid-Pleistocene [11].

1.2. Oceanography

Although no detailed oceanographic studies have been carried out specifically on Hatton Bank, various authors have described the characteristics of the main water masses observed in the easternmost part of the Iceland Basin, specifically bordering the western slope of Hatton Bank where the Hatton Drift is located (Figure 1). The contourite drifts are the result of sediments being transported and deposited by thermohaline bottom currents, dominated by the North Atlantic Deep Water (NADW). The origin of this bottom current relapse, on a large scale, in convection cells in the Labrador Sea and Norwegian Greenland Sea [14] and enters the Icelandic basin as an arm of the Deep Northern Boundary Current, which affects the western slope of the Hatton Bank and presents a cyclonic movement in the Icelandic Basin [15].

In the mid-latitude NE Atlantic Ocean, Van Aken [16] categorised the NADW in terms of four local source water types: Iceland–Scotland Overflow Water (ISOW); Lower Deep Water; Labrador Sea Water; and Mediterranean Sea Water. ISOW refers to the relatively salty water mass that travels westwards along the Iceland–Faeroe Slope and subsequently develops into the NADW (in addition to Denmark Strait Overflow Water and Labrador Sea Water, as the main water masses, with some mixture of Antarctic Bottom Water) [9,16–18].

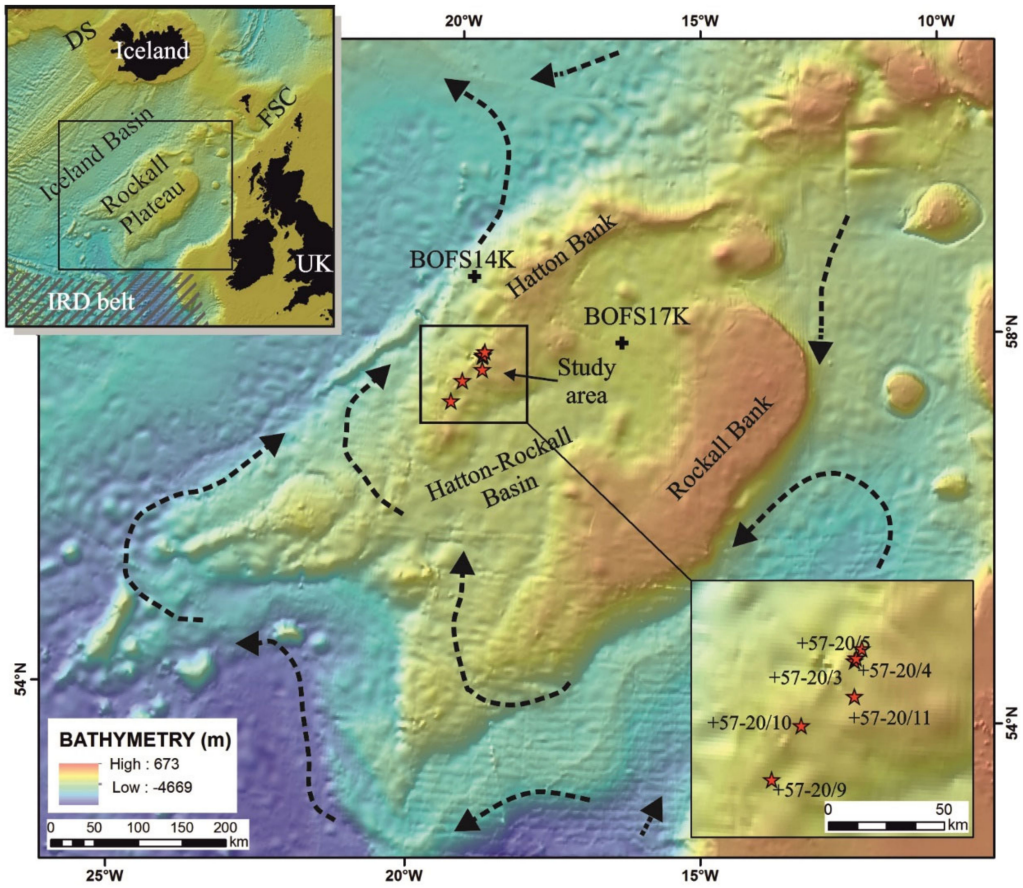

Figure 1. Local map showing the study area on Hatton Bank (northwestern part of the Rockall Plateau, NE Atlantic Ocean). Inset shows detailed location of the gravity cores. Dashed arrows show the main North Atlantic Deep Water (NADW) paths (of which Iceland–Scotland Overflow Water (ISOW) forms part) [9,16,17]. Locations of both sites BOFS14K and BOFS17K are shown (black crosses) [19–21]. Regional bathymetry from Amante and Eakins [22]. (UK: United Kingdom; IRD belt: Ice-Rafted Debris belt; DS: Denmark Strait; FSC: Faeroe–Shetland Channel).

1.3. Heinrich Events

Some studies show that fast climatic changes are related to coeval changes in the strength of the deep-sea circulation [23]. The apparent correlation between climatic and North Atlantic oceanographic records has led to speculation that these climate cycles exert intrinsic control in high latitudes and that ice-sheet–ocean–atmosphere interactions in the North Atlantic basin drive climate change elsewhere, through various feedback and amplification mechanisms [24].

In the North Atlantic, variation in sediment composition is largely dependent on the input of non-biogenic material from icebergs [25]. Heinrich events have been used not only to correlate cores across the Atlantic Ocean, but also to reconstruct the climatic and oceanographic conditions of the last 65 ka [19,23,26–31].

In sediments from the last glacial period (marine isotope stages—MIS—2–4), six episodes of increased Ice-Rafted Debris (IRD) can be observed across the North Atlantic [26,32,33]. These layers of IRD, known as Heinrich Layers (HL) [26,28,34], are found mainly in an area denominated the IRD belt [35]. This IRD belt extends in an arc from the Labrador Sea towards the Bay of Biscay, passing to the south of the Rockall Plateau (Figure 1). The layers were originated by Heinrich Events (HE) [26,36], defined as abrupt collapses of the Laurentidae ice-sheet (LIS) that delivered armadas of icebergs from Canada into the North Atlantic. These six brief time intervals (lasting a few hundred years [37,38]) have been labelled "H1" to "H6", from youngest to oldest, respectively [30,34,36], and Heinrich [26] demonstrated that they occurred approximately every 11 ka. However, Bard et al. [39] found HE effects

in sedimentary records beyond the IRD belt. Additionally, Bond and Lotti [27] demonstrated that the inputs of two other ice-rafted components (haematite-coated grains and basaltic glass), with different source areas, may slightly precede the detritial inputs from the LIS. In this research [27], authors found distinct peaks in three types; fresh, basaltic glass derived from Iceland, grains with hematite coatings (mostly quartz and feldspar) derived from any of the extensive red bed deposits in the region, and detritial carbonate grains that came mainly from carbonate rocks in eastern and northern Canada. The peaks rise above an ambient background composed mostly of quartz and feldspar and less than about 10% of grains with hematite coatings. In addition to the peaks in detritial carbonate at these levels of the Younger Dryas and H1, H2, and H4, they found a narrow peak of carbonate grains at the level of H3.

Several types of studies have been undertaken to detect these HE [20,23,26,29,30,32,40,41]. Four of the six HL, specifically H1, H2, H4 and H5, can be defined as "typical" HE (also named "cemented marls", in the sense of Hemming [30] and references therein), displaying distinct internal sedimentary patterns [42]. H4 has been reported as being the largest of the six events [36–38,43,44]. The main features of the H4 event as well as the main peaks in the graphs, are consistent with a large iceberg-derived freshwater flux and the associated retardation of the NADW [30,45–47]. Events H3 and H6 do not appear to have derived from the same sources as H1, H2, H4, and H5, and they have not been registered with confidence [30,44]. H3 and H6 have been described as low-foraminifera intervals rather than ice-rafting events [30].

All the studies indicate that there was large-scale disruption of the North Atlantic circulation, manifested in both surface and deep waters, correlating to the HE, due to the rapid influx of a large volume of freshwater (affecting Sea Surface Temperature (SST)), perturbations in thermohaline circulation (e.g., [48]), and which had enormous implications for climate [26,33,34]. There is convincing evidence that HL deposition was accompanied by the formation of a freshwater surface layer [36], which possibly stopped (or strongly reduced) NADW formation and thermohaline circulation [19,33].

Sediments from the site BOFS17K [19,20,30,49], located considerably further northwards of the main IRD belt (on Rockall Plateau at a water depth of 1150 m), were analysed for magnetic susceptibility (MS), foraminifera association, and SST, in order to reconstruct the activity of the NADW and the climate of the NE Atlantic in relation to HE. In addition, BOFS14K was analysed for magnetic susceptibility. Both sites are located close to the study area (Figure 1), which is considered a region of "moderate" IRD input during glacials [19–21]. Both cores (BOFS14K and BOFS17K) have been used to conduct studies establishing the MS signal of NE Atlantic sediments, as a proxy for their IRD content, in order to utilise this relationship in a palaeoceanographic context, mapping the variation in glacial/interglacial MS ratios for the Last Glacial Maximum (LGM) relative to the "most recent" Holocene [20].

Iceberg melting, which results in IRD accumulation, is characterised by the sequential deposition of high volumes of lithogenic material that can be identified using different proxies [19,20]. Detailed correlation of climatic proxies in North Atlantic sediment cores with Greenland ice core records provides a potential chronology for the HL, as well as global climate correlations [30,32]. Indeed, several studies have proposed the multiproxy approach as a reliable method for identifying HL and enabling palaeoclimate change reconstruction [20,23,27,29,30,37,44,50].

Based on the location and depth of the cores included in this research, it is believed that they represent the uppermost part of Hatton Drift. The overall aim of the study was to identify HE within a suite of gravity cores, using a multiproxy approach, in order to infer the age of these layers. In detail, the goals were (i) to characterise the main proxies for recognising HL by means of element enrichment/depletion, magnetic susceptibility (MS), and the grain size distribution relationship; (ii) to show which proxies are key for determining HE on Hatton Bank; (iii) to assign the age of each HE based on core correlation with the nearby BOFS17K and BOFS14K cores; and (iv) to estimate the mean sedimentation rate for glacial/interglacial periods in the study area.

2. Materials and Methods

Six gravity cores collected at around 1000 m water depth on Hatton Bank (Table 1) provide a detailed sedimentary record of glacial horizons as well as climatic and oceanographic variations during the Late Quaternary. The samples were obtained by the British Geological Survey (BGS, United Kingdom) on two cruises (1998 and 2009), and they have been studied under an agreement with the Instituto Español de Oceanografía (IEO, Spain). They have been analysed for magnetic susceptibility, geochemical composition, and grain size distribution (Appendix A, Table A1). In addition, micropaleontological studies of selected samples have been conducted on two of the cores (cores +57-20/9 and +57-20/10).

Table 1. Gravity cores studied in this work and collected from Hatton Bank. Latitude and longitude are taken from the BGS Offshore GeoIndex (https://www.bgs.ac.uk/GeoIndex/offshore.htm).

Core	Latitude (N)	Longitude (W)	Water Depth (m)	Length (m)
+57-20/3	57.8082	19.1988	951	0.48
+57-20/4	57.82083	19.1855	954	0.84
+57-20/5	57.8578	19.1497	972	0.81
+57-20/9	57.3285	19.7372	1041	2.04
+57-20/10	57.5451	19.5513	945	1.98
+57-20/11	57.6719	19.1831	933	1.47

The cores were split, photographed and described prior to sampling. The full length of the cores was analysed continuously at 1 cm resolution for magnetic susceptibility (MS), using a Bartington System MS2C sensor at the BGS laboratory. A 1-cm-thick sample was taken from each 5 cm interval for both textural and geochemical analyses. The grain size distribution was recorded using a Horiba Partica LA-950V2 laser diffraction particle size analyser at the Institute of Marine Sciences-CSIC, in Barcelona; the > 2 mm fraction was sieved and taken into account to determine the total grain size distribution. Samples for geochemical analysis were powdered in an agate grinder and then analysed at Acme Analytical Laboratories Ltd. (Canada). The method chosen was the so-called 4-acid digestion technique, to achieve a full suite of 43 elements and rare earth elements through Inductively Coupled Plasma Mass Spectrometry (ICP-MS). In order to correct element concentrations for carbonate dilution and grain-size effects, Ca- and Al-normalisation have been applied, respectively. In addition, five selected samples were taken from both the +57-20/9 and +57-20/10 cores for foraminiferal description to support the facies characterisation.

3. Results

The main results of this research are given in three different sections: (i) the main facies that characterise the cores; (ii) the change-tendency of the main proxies; and (iii) a semi-quantitative study of the foraminifera associations.

3.1. Sediment Facies

The cores present interbedded facies of calcareous ooze (F1) and lithogenous silt (F2). These two main facies can be defined in the study area based on the relative proportions of two major sedimentary components: carbonate muddy sand and siliciclastic mud, respectively, which are sometimes bioturbated (showing a sharp color change). In general, F1 comprises white (Munsell Colour System 10YR8/1) to light yellowish brown (10YR6/4) muddy sand, with predominant tests of planktonic foraminifera, in addition to some quartz grains, sponge spicules, and lithic fragments; while F2 is characterised by light olive-brown (2.5Y5/4) mud mainly comprising silt-sized sediments of quartz grains, dark minerals, small rock fragments, and some planktonic foraminiferal tests (low-moderate presence).

The granulometric distribution of each facies is completely different (Figure 2). Sample +57-20/9 (160−161 cm) places the sediment of F1 in the field of the muddy-sand textural group [51]. According to the Folk and Ward method (1957) [52], the sediment is very poorly sorted (2.6 Ø) displaying a bimodal grain size distribution with the principal mode being very fine sand—3.1 Ø (115.1 µm)—very close to the median value (3.5 Ø). The F2 type sample, +57-20/9 (140−141 cm), fits within the mud textural group, and is characterised by a polymodal distribution of very poorly sorted material (2.3 Ø), dominated by very fine silt, with a median grain size value of 7.3 Ø (6.3 µm).

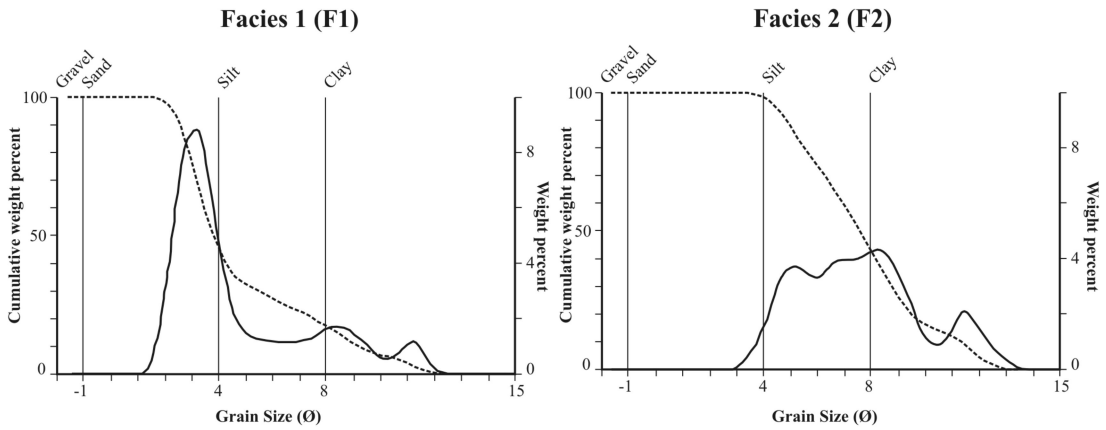

Figure 2. Typical granulometric distribution of the two main facies described in this work: Facies 1: sample +57-20/9 (160−161 cm) of calcareous ooze (**F1**); and Facies 2: +57-20/9 (140–141 cm), lithogenous silt (**F2**).

3.2. Proxies

Some element/Ca ratio indices such as Mg/Ca, Fe/Ca, and Al/Ca give prominent and consistent trend peaks versus depth over a regular background ratio, following a similar pattern to that of the MS signal. Coincident with these tendencies, silt and REE/CC (Rare Earth Elements normalised by Continental Crust [53]) peaks are also observed. Five restricted depth intervals have been recognised in the cores, and these peaks relate to alternating dominance of calcareous and lithogenic facies (Figure 3). In addition, some palaeoproductivity proxies, such as Cd/Al, Ba/Al, and P/Al, show, in general, opposing tendencies to those observed in the lithogenic proxies in the cores (Figure 3).

3.3. Foraminifera Associations

Only two cores (+57-20/9 and +57-20/10) were studied for foraminifera associations, based on the semi-quantitative data shown in Table 2. Five samples were analysed for each core. The samples were examined for calcareous microfossils in order to determine whether any environmental variability could be recognised. In general, benthonic foraminifera were rare and patchily distributed, whereas planktonic foraminifera were abundant.

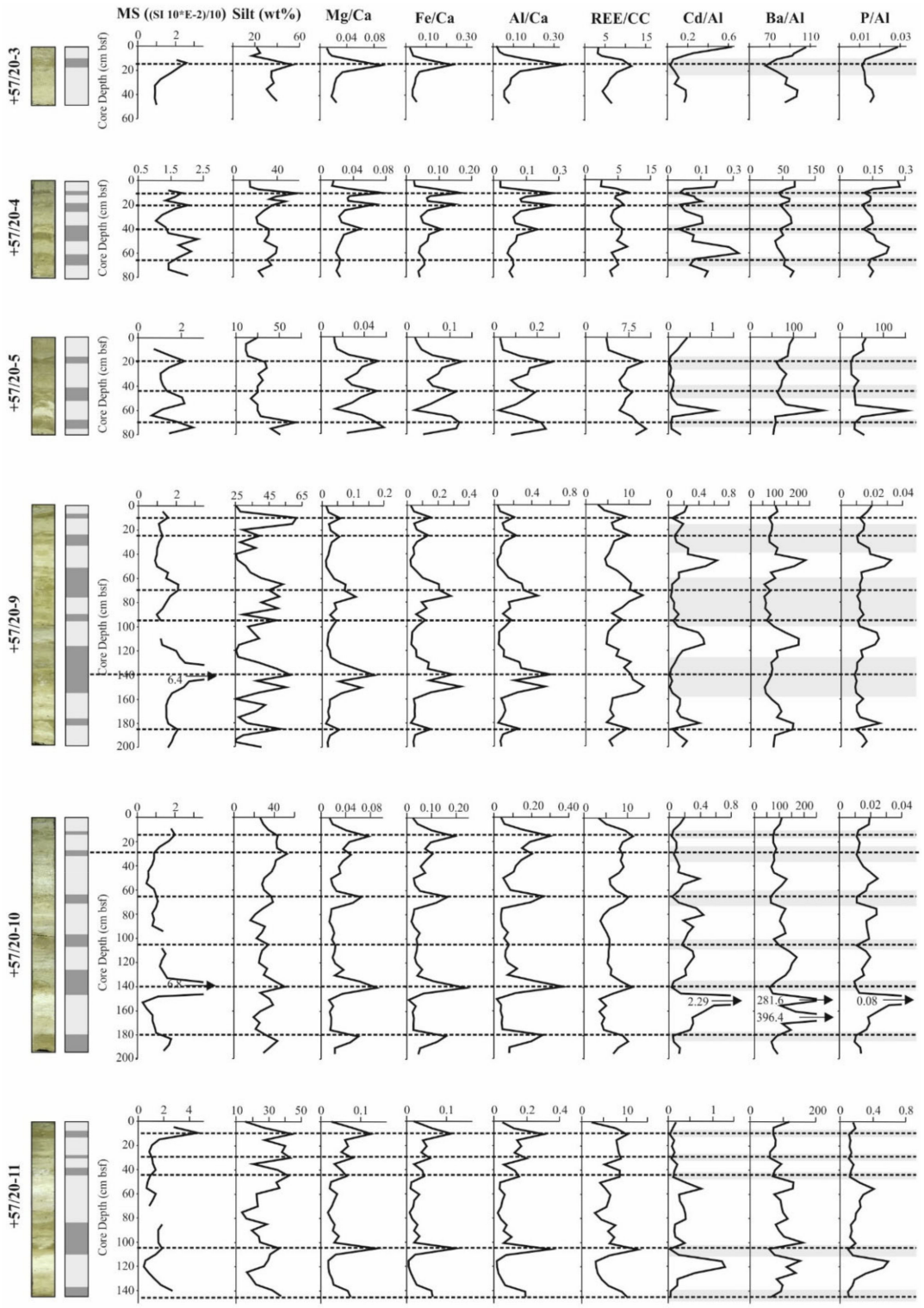

Figure 3. Main results from the gravity cores, as well as the position of prominent peaks (dashed lines) established in this study. From left to right, photograph next to the interpreted sketch based on the two facies described in this study: F1: calcareous ooze (light grey) and F2: lithogenous silt (dark grey). Depth profiles of magnetic susceptibility (MS), silt, Mg/Ca, Fe/Ca, Al/Ca, and REE/CC (Rare Earth Elements normalised by Continental Crust [53]). Depth profiles of palaeoproductivity proxies (Cd/Al, Ba/Al, P/Al) where the grey areas show ratio depletions coincident with the dashed lines.

Table 2. Distribution of microfossils in cores +57-20/9 and +57-20/10 (based on BGS internal report [54]). SQ: Semi-quantitative.

+57-20/9				
Depth (bsf)	**Benthonic Foraminifera**		**Planktonic Foraminifera**	
	Species	**SQ data**	**Species**	**SQ data**
0.09 m	*Gaudryina* sp.	Rare	*Neogloboquadrina pachyderma (s)*	Abundant
	Lenticulina sp.	Rare	*Globigerina bulloides*	Abundant
	Planispirinoides buccelentus	Rare	*Globorotalia inflata*	Common
	Quinqueloculina sp.	Rare		
	Sigmoilopsis schlumbergeri	Rare		
0.46 m	?	Very rare	*Orbulina universa*	Rare [a]
			Globorotalia truncatulinoides	Rare
			Globorotalia scitulus	Rare
			Globigerina bulloides	Abundant
			Globorotalia inflata	Common
			Neogloboquadrina pachyderma (s)	Rare
1.09 m	*Gaudryina* sp.	Rare	*Orbulina universa*	Rare [a]
	Lenticulina sp.	Rare	*Globorotalia scitulus*	Rare
	Planispirinoides buccelentus	Rare	*Globorotalia truncatulinoides*	Rare
	Quinqueloculina sp.	Rare	*Globigerina bulloides*	Abundant
	Sigmoilopsis schlumbergeri	Rare	*Globorotalia inflata*	Abundant
1.35 m [b]		Barren	*Globigerina bulloides*	1 specimen [c]
			Neogloboquadrina pachyderma (s)	4 specimens [c]
1.74 m	*Gaudryina* sp.	Rare	*Orbulina universa*	Rare [a]
	Lenticulina sp.	Rare	*Globorotalia scitulus*	Very rare
	Planispirinoides buccelentus	Rare	*Globorotalia truncatulinoides*	Very rare
	Quinqueloculina sp.	Rare	*Globigerina bulloides*	Common
	Sigmoilopsis schlumbergeri	Rare	*Globorotalia inflata*	Abundant
			Neogloboquadrina pachyderma (d & s)	Very rare
+57-20/10				
Depth (bsf)	**Benthonic foraminifera**		**Planktonic foraminifera**	
	Species	**SQ data**	**Species**	**SQ data**
0.1 m	*Cibicides refulgens*	Rare	*Neogloboquadrina pachyderma (s)*	Abundant
	Rupertina stabilis	Rare	*Globigerina bulloides*	Frequent
	Pyrgo sp.	Rare		
	Quinqueloculina sp.	Rare		
	Sigmoilopsis schlumbergeri	Rare		
0.49 m	*Laticarinina pauperata*	Rare	*Globigerina bulloides*	Abundant
	Cibicides refulgens	Rare	*Globorotalia inflata*	Frequent
	Eggerella propinqua	Very rare	Ostracoda: *Echinocythereis* sp.	Very rare
	Sigmoilopsis schlumberger	Rare		
	Melonis barleeanum	Very rare		
1.24 m	*Pyrgo* sp.	Rare	*Orbulina universa*	Rare [d]
	Quinqueloculina sp.	Rare	*Globigerina bulloides*	Rare
	Uvigerina peregrina	Rare	*Globorotalia inflata*	Frequent
	Cibicidoides sp.	Rare	*Globorotalia scitulus*	Rare
	Spiroloculina sp.	Rare	*Neogloboquadrina pachyderma (d & s)*	Frequent
	Trifarina angulosa	Rare		
1.43 m [e]	*Sigmoilopsis schlumbergeri*	Rare	*Globigerina bulloides*	Frequent
	Cibicides sp.	Rare	*Globorotalia inflata*	Rare
	Cibicidoides sp.	Rare	*Neogloboquadrina pachyderma (s)*	Frequent [f]
			Indeterminate planktonics	Common

Table 2. *Cont.*

1.53 m	*Sigmoilopsis schlumbergeri*	Rare	*Orbulina universa*	Very rare
	Paromalina coronata	Rare	*Globorotalia scitulus*	Rare
	Pyrgo sp.	Rare	*Globorotalia truncatulinoides*	Very rare
	Cibicides sp.	Rare	*Globigerina bulloides*	Abundant
			Globorotalia inflata	Abundant

[a] Small and medium sized. [b] Foraminifera were very rare. [c] Small. [d] Small. [e] Slightly sandier compared to above and below. Preservation poor- mainly fragmentary. Forams common, but only in the 125-micron sieve and fines pan. The presence of small individuals only may be the result of current activity and winnowing. [f] Mainly sinistral but also dextral.

4. Discussion

4.1. Age-Model Based on Identification of Heinrich Events

Studies of North Atlantic cores show a strong correlation between variations in the MS signal and the lithological composition of the sediments. For this reason, changes in MS measurements in the study area may reflect changes in the amount and type of detritial input. The MS peaks provide evidence of increased concentrations of magnetic minerals coinciding with an augmented silt concentration (Figure 3). In the North Atlantic, authors usually define MS peaks close to peaks in coarse material during cold stages, related to IRD input [55,56] but some studies have proven that the sediments are reworked by bottom currents and, in consequence, significant concentrations of IRD could also be observed in finer fractions [28,30], as may be reflected in this study. The presence of IRD in sediments is connected with HL and, therefore, HE [26,32–34,57].

As the results from all six cores show similar patterns, based on the analyses performed (Figure 3), core +57-20/9 is shown in detail, as it is representative of all the cores, but also because is the longest and it is well preserved. Comparing the MS of core +57-20/9 with the reference cores BOFS14K and BOFS17K [20], from locations close to the study area (Figure 1), should allow us to correlate the major parameter peaks of the HE and ash events; BOFS17K has also been dated for HE1 to HE6 [30,49]. Therefore, based on the evidence of the H4 record and by comparing this with the BOFS14K and BOFS17K sites, we are able to correlate one ash layer as well as HL: H1, H2, H4, and H5 (Figure 4).

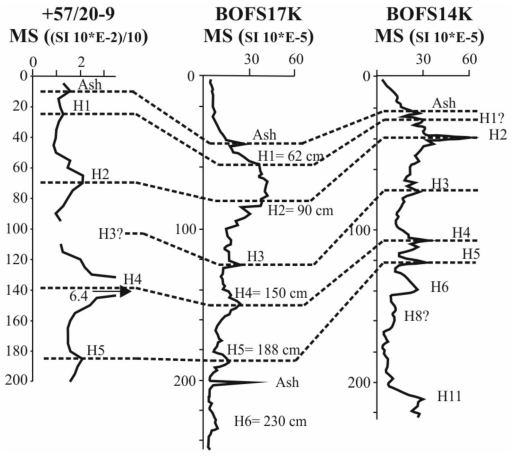

Figure 4. Comparison of MS between depth profiles from the three sites: +57-20/9 core (this work), BOFS17K, and BOFS14K (modified from [20,30,49]). See Figure 1 for location.

Based on the information available for BOFS17K and BOFS14K, the most recent event is associated with an ash layer. The information obtained in this study reveals an analogous peak, categorised as an ash layer (for comparison), although the presence of tephra shards has not yet been confirmed. Some studies support ash layer detection based on MS analyses [20,58–62]. The ash layer is likely to be Ash Zone I [5,63], which occurs within the Younger Dryas (YD) [58,64]. This ash layer may include the

Vedde Ash, an important volcanic event marker layer characterised by a higher Fe content than other Icelandic ashes [64], facilitating the correlation of terrestrial to marine sequences in Europe and the North Atlantic [65]. The Vedde Ash event is believed to have derived from an eruption of the Katla volcano in Iceland that occurred during the YD, at around 12.1 ka BP [65].

Some indices, e.g., Fe/Ca, have been proposed as proxies for drastic changes in sedimentation, relating to HE in the Atlantic Ocean [50,56,66–68]. In every HL, it is possible to observe an initial increase in the element/Ca ratio, which gradually decreases toward the end of a HE. In light of the results of this work, it can be seen that the Mg/Ca, Fe/Ca, Al/Ca, and REE/CC indices, as well as silt content, produce prominent and consistent peaks that match the alternating dominance of the calcareous and lithogenic facies (Figure 5). As consequence, the sediment displays a high percentage of carbonate (mainly foraminiferal tests and shell fragments) in warm periods, compared to the lithogenic-dominated composition (small rock fragments of various origins) seen during cold stages.

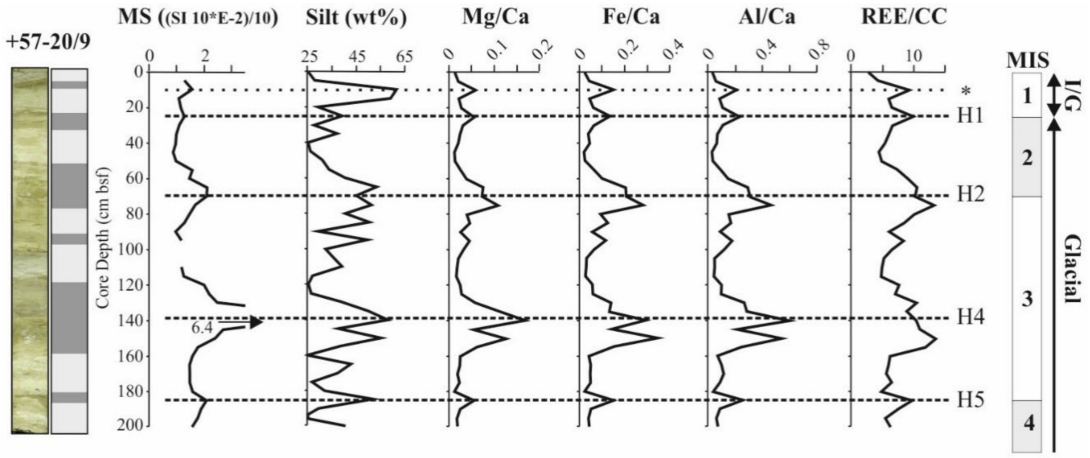

Figure 5. Inferred position of Heinrich events (dashed lines) based on the main proxies and sediment facies for Core +57-20/9. The ash layer (*) is also highlighted (dotted line). The events are marked in the centre of the layers and do not cover the entire layer thickness. From left to right: photograph next to the interpreted sketch based on the two facies described in this study (F1: calcareous ooze (light grey) and F2: lithogenous silt (dark grey)) and depth profiles of proxies studied. (I/G, Interglacial/Glacial transition).

A chronology for the sedimentary record of Hatton Bank has been obtained based on detection of HL. According to the calibrated ages established for these cold events [30,36,37,44], the HL identified would have the following ages: 17.5 ka BP (H1); 25.15 ka BP (H2); 31.2 ka BP (H3); 43.1 ka BP (H4); and 54 ka BP (H5). This approach provides an age-model that has been developed following the same method used for core +57-20/9 and applying to all the cores included in this work. The proposed age-model for each of the six cores studied is shown in Table 3.

Table 3. Age-model proposed in this work based on the six cores studied. Calibrated age based on studies by other authors [37,44,65].

AGE (cal ka BP)	HE	DEPTH (cm bsf)					
		+57-20/3	+57-20/4	+57-20/5	+57-20/9	+57-20/10	+57-20/11
12.1	Ash/YD	15	10	20	10	15	10
17.5	H1	-	20	20	25	30	30
25.15	H2	-	40	45	70	65	45
31.2	H3	-	65	75	95	105	105
43.1	H4	-	-	-	140	140	-
54	H5	-	-	-	185	190	-

In the study area, the Fe/Ca and MS peaks, in particular, may indicate basalt content (from Iceland), provided by ice-rafting, and which may have been transported and redistributed by bottom currents (mainly ISOW as part of the NADW) from the basaltic province Faeroe–Shetland Channel [23,29]. Deep sea currents were enhanced/reduced during the interstadials/stadials transporting magnetic particles from the Norwegian Sea into the North Atlantic Ocean along a path similar to the present trajectory of the NADW [23,29]. Some authors [23,29,69–71] suggest that the Faeroe–Shetland Channel and the Denmark Strait were the only two active pathways for the overflow water. In addition, Peck et al. [72] showed the potential of coupled Fe/Ca-MS variation records as preliminary indicators of HL and ash layers in sediment cores, an assumption which could explain a peak identified as an ash layer in this study.

The most prominent peak in the +57-20/9 core (Figures 3 and 5) was observed at a depth of ~140 cm; this was assigned with particular confidence as Heinrich layer H4, since it is the largest of the six events during the last glacial period [30,37]. There is evidence for various IRD sources regions in H4 as North America, Iceland, Greenland and Europe [28,32,36,41,72–74]. It is known that the LIS (Laurentidae Ice Sheet in Canada) was the dominant source of IRD within the North Atlantic [32,37,73], but there is also evidence suggesting a European contribution [30,41,42,62,75]. Provenance studies indicate that there were pulses just prior to many HL, sourced from Greenland and European ice sheets rather than the LIS [75]. In this sense, and based on the results of this study, a coeval variation of Mg and Fe curves can be observed, except in H4 where two separate peaks occur in some cores (Figure 6); in cores +57-20/9 and +57-20/10, H4 is characterised by a first increase of Fe and Mg, at ~150 cm, and then a second increase of just Mg content, at ~135 cm. This particular record may be explained by the deposition of a European precursor enriched in basalt (peak Fe-enrichment at ~150 cm) from the FSC, which is then overlain by Mg-rich dolomitic material (peak Mg-enrichment at ~135 cm) from the LIS transported by icebergs from Canada. Both cores are from south of core +57-20/11 (Figure 1), where this decoupling signal between Fe and Mg is not detected. Thus, it can be suggested that the northernmost boundary where the occurrence of HE can be recorded is around 57°38′ N in the Hatton–Rockall area, northwards of the present day IRD belt, at least for H4, as this is the largest event and most confidently recognised in the area. This fact corroborates the northern boundary proposed by Rassmunsen and Thomsen [76], who defined a Heinrich belt with a northern limit at around 58−60° N in the same area.

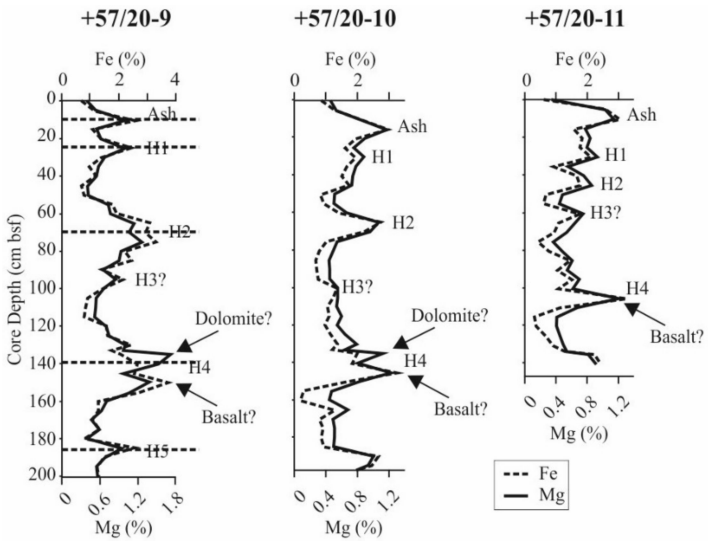

Figure 6. Depth profile of Fe and Mg content in three sediment cores from the study area where decoupling peaks of these elements in H4 are assigned to their possible origin, i.e., basalt (Fe) or dolomite (Mg).

The palaeoproductivity proxies (Cd/Al, Ba/Al, and P/Al) in these cores also support the identification of HE in this study. They show an increase just before the onset of a HE, followed by

a minimum during the HE itself (Figure 3). The study of Hinrichs et al. [44] shows an increase in sediment components, such as Ba content, both before and during HE in a core collected to the south of the study area. Similarly, P/Al and Cd/Al were used as palaeoproductivity proxies indicating upwelling activity [77]. The increase in palaeoproductivity tracers in the sedimentary record has been interpreted to reflect reduced NADW formation and the consequent northward penetration of nutrient-rich waters from the South Atlantic [78].

In addition, and based on the microfaunal analyses of cores +57-20/9 and +57-20/10, the calcareous microfossil assemblage of the cores is dominated by planktonic foraminifera while benthic foraminifera are rare and unevenly distributed (Table 2). In general, the observed assemblages point to cooling environmental conditions [54] from the base toward the top of the cores—in an expansion of Arctic conditions (water temperatures below 7 °C) southwards—at least until the sample recovers, at ~10 cm, after which there is warming up to the present day. These results may reflect the cooling trend from ancient to recent times, a fact that matches the climate environment described between H4 and the ash layer (or YD), and a subsequent warming trend (up to the conditions of the present day).

4.2. Chronostratigraphic Approximation and Reconstruction

Based on the depth variation of the proxies and the estimated chronostratigraphy for the six cores retrieved from Hatton Bank, we have been able to reconstruct the HE (Figure 7) in an area outside the IRD belt (maximum HE deposition). It is worth noting that the bioturbation observed in H2 could be used as an additional proxy for correlating this HE between the cores.

When plotting these HE ages versus core depth (Figure 8), a mean sedimentation rate of 1.5 cm ka^{-1} for the last ~18 ka (interglacial), and 4.3 cm ka^{-1}, for the last glacial, can be estimated.

In order to verify the correlation proposed in this work, the sedimentation rates have also been calculated for all the cores included in this study and compared with other nearby studied cores (Table 4). In this way, mean sedimentation rates of 1.4 cm ka^{-1} for the last interglacial period (~18 ka), and 4.2 cm ka^{-1} for the last glacial period, have been obtained. To support these estimations, the sedimentation rates of BOFS14K and BOFS17K have also been calculated based on data reported by several authors [19,20,30], as these are located within the vicinity of the study area. The results obtained are comparable to those of Thomson et al. [37] and Hinrichs et al. [44], although with higher values for more proximal areas of the NE Atlantic. Thereby, the values show similar magnitudes (although differences in sedimentation rates may be due to the study area being far from any continental input, in addition to the water depth of the different core locations), which supports the chronostratigraphy proposed in this work.

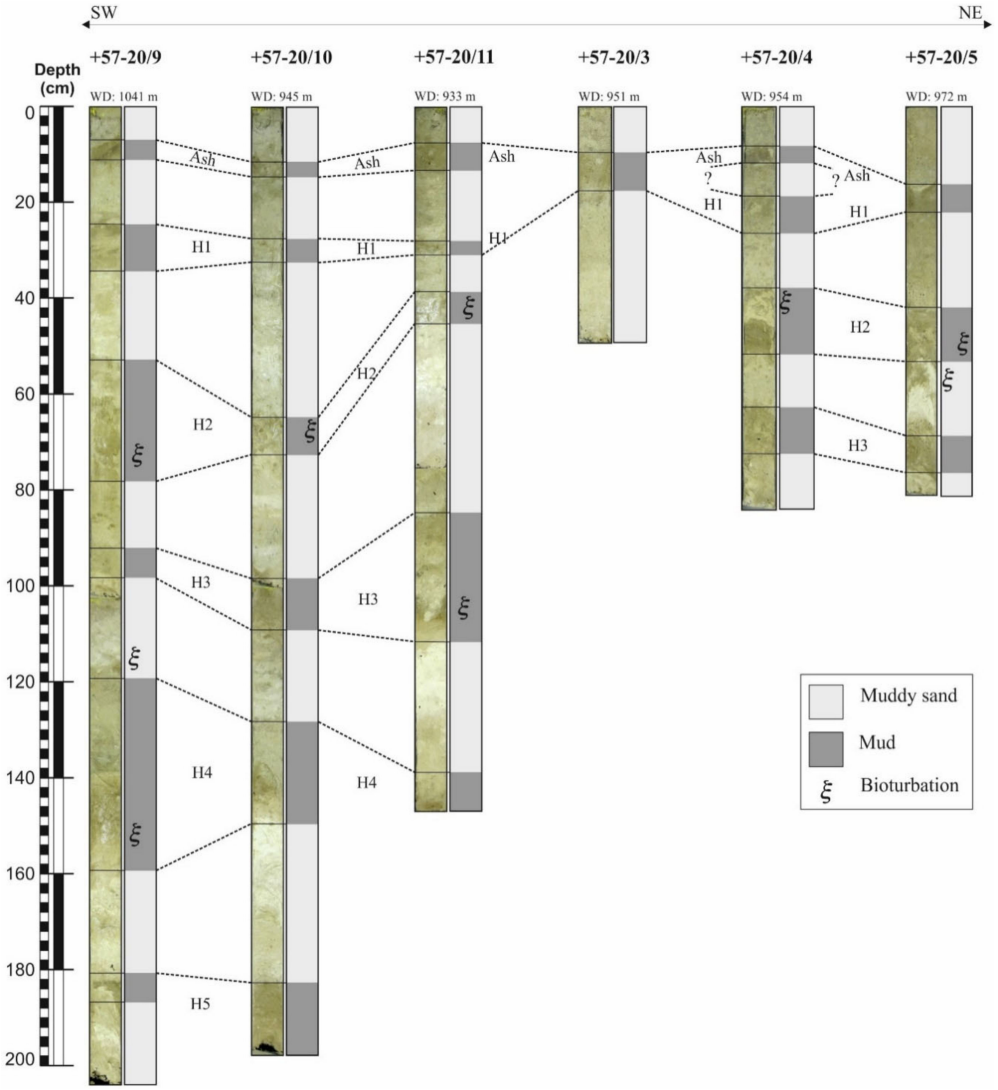

Figure 7. Correlation plot of the six gravity cores studied from the Hatton Bank–Rockall Plateau where the ash layer and Heinrich Events (HE) identified in this study are shown. Two columns are plotted for each gravity core: picture on the left side and an interpretation sketch on the right side.

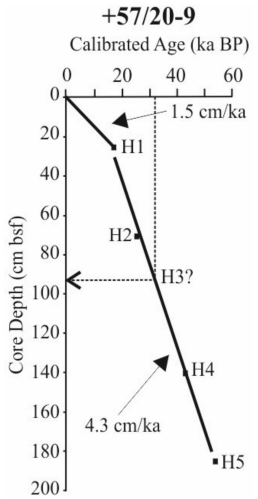

Figure 8. Sedimentation rates based on the correlation between the HL identified in the +57/20-9 core and the published calibrated ages for the HE [30,36,37,44]. Two lineal regressions have been calculated to obtain sedimentation rates depending on the climatic period.

Table 4. Sedimentation rates calculated for the NE Atlantic.

Reference	Study Area	Water Depth	Mean Sedimentation Rates	
			Interglacial	Last Glacial
Hinrichs et al., 2001 [44]	Station Bengal (SW British Isles)	4804 m	2.1 cm ka^{-1}	5.4 cm ka^{-1}
Thomson et al., 1995 [37]	Armorican Seamount (W British Isles)	3849 m	2.2 cm ka^{-1}	5.6 cm ka^{-1}
Calculations based on Maslin et al., 1995 [19], Robinson et al., 1995 [20]	Western Slope Hatton Bank (BOFS14K)	1756 m	1.4 cm ka^{-1}	2.9 cm ka^{-1}
Calculations based on Maslin et al., 1995 [16], Robinson et al., 1995 [20], Hemming, 2004 [30]	Hatton–Rockall Basin (BOFS17K)	1150 m	3.5 cm ka^{-1}	3.4 cm ka^{-1}
This work	Hatton Bank	~1000 m	1.4 cm ka^{-1}	4.2 cm ka^{-1}

In addition, the typical HL (H1, H2, H4, and H5) have been defined as being primarily sourced from LIS, whereas H3 is an atypical HE (as is H6, although it is not covered in this study) that seems to be derived from European sources, making more it difficult to recognise due to different IRD compositions [30,73,79]. Furthermore, H3 shows only a weak MS signal in both BOFS14K and BOFS17K (Figure 4). The results of this work allow estimating an age of 31.2 ka (H3) and a depth of ~95 cm for H3, taking into account the ratio calculated for the +57-20/9 gravity core (Figure 8). This depth is coincident with most of the weak peaks observed for other proxies, such as silt, Mg/Ca, Fe/Ca, Al/Ca, and REE/CC (Figure 9).

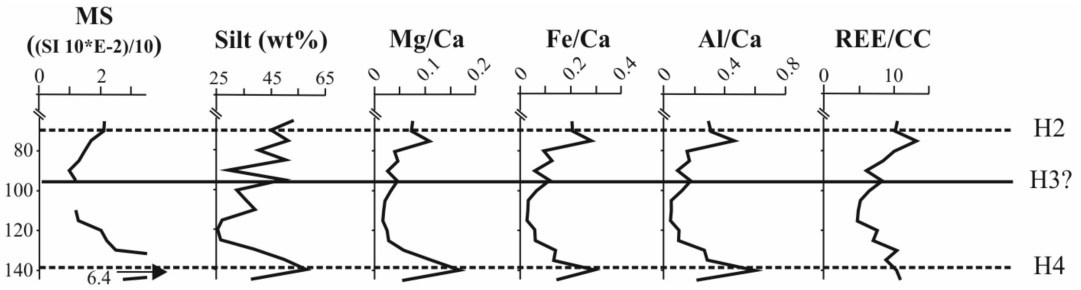

Figure 9. A detailed range of depth profiles for the ratios studied in +57-20/9 (see Figure 5), showing a possible H3 signal (solid line). H2 and H4 are marked with dashed lines.

5. Conclusions

The study of six gravity cores from the Hatton Bank–Rockall Plateau beyond the IRD belt (NE Atlantic areas where HE deposition was the most intense) reveals that peaks from the MS signal, silt content, Mg/Ca, Fe/Ca, Al/Ca, and REE/CC, are sensitive proxies for HE (H1, H2, H3, H4, and H5). This is supported by an increase in palaeoproductivity proxies (Cd/Al, Ba/Al and P/Al) before/during typical HE (H1, H2, H4, and H5). The decoupling behaviour of Fe and Mg (%) in some sediment layers may allow different source areas for the HE to be distinguished, since the sediments deposited are from different provenances, i.e., the basaltic province of the FSC and/or dolomite-rich material from the LIS. For this reason, Fe content and MS have been proposed as good proxies for detecting HE and ash layers in the Hatton Bank deposits. Identifying HE after applying these proxies has allowed to: (i) establish an age-model for the six cores; (ii) approximate the chronostratigraphy; and (iii) estimate the mean sedimentation rates for the last glacial (~4.2 cm ka^{-1}) and interglacial (~1.4 cm ka^{-1}) periods in the area, revealing fairly uniform deposition of HE from between water depths of 933 and 1041 m.

The results of this work suggest that the northernmost boundary where HE are recorded is located around 57°38′ N in the Hatton–Rockall area, northwards of the present day IRD belt, at least for H4 (the largest event), based on the variations in the Mg/Ca and Fe/Ca curves.

In general, the layers with prominent lithic-rich and foraminifera-poor sediments, established as Heinrich layers, may be related to iceberg melting and an injection of freshwater that could have reduced the formation of NADW. This would have had an important impact on the thermohaline circulation around the Hatton Bank–Rockall Plateau, since this current is one of the main components of the system. During the period with reduced NADW activity, more fine-grained sediments (mainly silt) were deposited, because the material transported by bottom currents, predominantly comprising basalt (and other terrigenous components), was principally eroded from FSC (or areas close to the European margin) and was transported by the ISOW. In this sense, the MS record in the Hatton Bank sediments could be a good parameter for inferring strengthened/weakened NADW formation, according to whether they were deposited during a stadial or an interstadial. As a consequence of the reduced NADW flow, water from the South Atlantic (nutrient-rich waters) penetrated northwards, evidenced by an increase in the main palaeoproductivity proxies, that decrease once again towards the next Heinrich event.

Author Contributions: Conceptualization, M.S.-G. and N.L.-G.; methodology, M.S.-G., N.L.-G. and D.L.; writing—original draft preparation, M.S.-G.; writing—review and editing, M.S.-G., N.L.-G., D.L., L.M.F.-S. and P.D.-M.; supervision, M.S.-G., N.L.-G., D.L., L.M.F.-S. and P.D.-M.; project administration, L.M.F.-S. and P.D.-M.; funding acquisition L.M.F.-S., P.D.-M. and D.L. All authors have read and agreed to the published version of the manuscript.

Funding: This research was carried out as part of the Ecovul/Arpa project, Instituto Español de Oceanografía (IEO) and Secretaría General del Mar (SGM), Spain. The study received financial support from the IEO, British Geological Survey (BGS), Andalusian Regional Government (PAI), and a FPI grant (IEO supported).

Acknowledgments: Thanks are especially due to the sedimentological research group of the CMIMA-CSIC for the grain size analyses. We would also like to show our appreciation to the BGS for their support. Our most sincere thanks go to K. Hitchen for his help and enthusiasm.

Conflicts of Interest: The authors declare no conflict of interest.

Appendix A

Table A1. Results of all the samples from the six gravity cores studied for geochemical composition and grain size distribution.

Samples	Fe (%)	Cd (ppm)	Ca (%)	P (%)	Mg (%)	Ba (ppm)	Al (%)	Total_REE (CC)	Gravel (%)	Sand (%)	Silt (%)	Clay (%)
57-20/3 0–1	0.69	0.57	33.39	0.020	0.35	78	0.74	3.13	0.00	73.64	22.06	4.31
57-20/3 5–6	0.84	0.35	28.35	0.022	0.41	103	1.10	2.97	0.00	71.16	25.19	3.65
57-20/3 7–8	0.98	0.34	26.55	0.025	0.49	138	1.50	4.09	0.00	79.59	17.88	2.54
57-20/3 10–11	2.13	0.30	21.85	0.040	0.93	257	3.35	8.59	7.00	45.58	32.97	14.46
57-20/3 15–16	3.07	0.25	13.71	0.050	1.24	316	4.80	10.56	0.00	29.99	53.53	16.48
57-20/3 20–21	1.47	0.30	21.04	0.034	0.72	229	2.95	7.41	0.00	40.71	35.25	24.04
57-20/3 25–26	1.17	0.34	23.58	0.027	0.60	200	2.30	5.87	0.00	47.55	34.88	17.57
57-20/3 30–31	1.12	0.22	24.12	0.026	0.56	183	2.14	5.27	0.00	50.53	37.36	12.12
57-20/3 35–36	0.88	0.36	26.43	0.024	0.54	155	1.60	4.12	0.00	56.95	30.58	12.47
57-20/3 40–41	0.88	0.40	27.14	0.027	0.50	162	1.69	5.00	0.00	46.07	35.16	18.77
57-20/3 45–46	1.31	0.48	24.88	0.032	0.62	192	2.26	6.26	0.00	36.35	40.61	23.04
57-20/4 0–1	0.72	0.23	30.99	0.021	0.51	94	0.92	3.43	0.00	82.44	14.61	2.96
57-20/4 5–6	0.79	0.22	30.86	0.022	0.44	95	0.93	3.21	0.00	81.73	15.38	2.90
57-20/4 7–8	1.74	0.21	22.85	0.034	0.80	214	2.56	6.67	0.00	70.94	22.64	6.42
57-20/4 10–11	2.59	0.27	15.90	0.042	1.20	281	4.27	9.68	0.00	25.19	58.25	16.57
57-20/4 13–14	1.51	0.39	20.68	0.036	0.75	215	2.94	6.81	0.00	38.91	38.61	22.48
57-20/4 15–16	1.34	0.37	21.68	0.032	0.73	235	2.58	6.59	0.00	39.87	33.76	26.38
57-20/4 17–18	1.45	0.48	22.16	0.033	0.76	253	2.78	7.61	0.00	19.22	48.01	32.77
57-20/4 20–21	2.13	0.25	14.74	0.035	0.98	272	3.94	8.55	0.00	44.16	35.84	20.01
57-20/4 25–26	1.39	0.23	21.32	0.027	0.65	212	2.58	6.27	0.00	61.40	27.68	10.92
57-20/4 30–31	1.02	0.34	22.44	0.025	0.52	185	1.98	5.57	0.00	64.94	21.31	13.75
57-20/4 35–36	1.14	0.38	22.11	0.028	0.58	202	2.14	6.21	0.00	59.75	22.37	17.88
57-20/4 40–41	1.98	0.20	18.18	0.034	0.90	249	3.62	8.20	0.00	48.04	32.46	19.50
57-20/4 45–46	1.65	0.33	24.14	0.034	0.70	193	2.53	8.15	0.00	55.80	31.82	12.38
57-20/4 50–51	1.71	0.33	26.47	0.038	0.68	153	2.64	7.03	1.19	54.65	28.50	15.66
57-20/4 55–56	1.25	0.67	29.49	0.042	0.65	134	2.16	9.56	3.60	23.21	40.31	32.89
57-20/4 60–61	1.07	0.62	28.47	0.032	0.56	125	1.74	5.84	0.00	35.26	39.46	25.28
57-20/4 65–66	1.50	0.32	27.70	0.029	0.66	188	2.38	6.72	1.03	53.95	31.12	13.91
57-20/4 70–71	1.57	0.29	28.46	0.029	0.67	200	2.55	7.35	0.00	53.32	35.57	11.12
57-20/4 75–76	0.97	0.38	26.91	0.025	0.53	187	1.87	5.40	2.20	61.78	23.14	12.88
57-20/4 80–81	1.01	0.39	24.31	0.025	0.59	194	2.11	5.94	6.06	58.01	27.63	8.30
57-20/5 0–1	0.58	0.48	32.70	0.018	0.39	85	0.80	3.30	0.00	62.28	30.73	7.00

Table A1. *Cont.*

Samples	Fe (%)	Cd (ppm)	Ca (%)	P (%)	Mg (%)	Ba (ppm)	Al (%)	Total_REE (CC)	Gravel (%)	Sand (%)	Silt (%)	Clay (%)
57-20/5 5–6	0.72	0.39	31.54	0.018	0.41	86	0.89	3.37	0.00	76.23	19.27	4.51
57-20/5 10–11	1.08	0.33	32.76	0.024	0.48	108	1.15	3.61	0.00	77.99	19.16	2.86
57-20/5 15–16	1.40	0.24	23.76	0.028	0.61	219	2.41	5.97	0.00	73.43	21.17	5.41
57-20/5 20–21	2.30	0.24	18.27	0.039	0.95	253	4.00	8.81	0.00	44.28	36.90	18.82
57-20/5 25–26	1.57	0.28	19.59	0.027	0.74	199	2.71	6.45	0.00	42.38	38.57	19.05
57-20/5 30–31	1.35	0.19	18.87	0.025	0.63	218	2.47	6.02	0.00	55.77	31.24	12.99
57-20/5 35–36	1.15	0.31	24.43	0.026	0.57	126	1.62	5.31	0.00	56.50	34.96	8.54
57-20/5 40–41	1.35	0.36	22.58	0.026	0.64	159	2.15	5.71	0.00	57.40	30.11	12.49
57-20/5 45–46	2.15	0.31	19.17	0.037	0.99	198	3.01	7.17	0.00	54.26	30.26	15.49
57-20/5 50–51	1.60	0.36	19.71	0.033	0.73	181	2.46	6.23	0.00	59.95	23.75	16.31
57-20/5 55–56	1.26	0.59	23.20	0.028	0.66	173	1.99	5.88	0.00	42.75	30.14	27.12
57-20/5 60–61	0.51	0.86	30.47	0.036	0.40	107	0.60	5.30	0.00	23.79	29.92	46.29
57-20/5 65–66	1.95	0.33	19.14	0.042	0.73	136	2.22	7.23	1.36	44.64	33.00	21.00
57-20/5 70–71	2.04	0.33	16.87	0.039	0.83	189	3.03	7.99	0.00	7.61	64.70	27.69
57-20/5 75–76	2.01	0.45	17.66	0.044	1.02	202	3.51	9.34	0.00	20.99	42.20	36.81
57-20/5 80–81	0.93	0.70	25.48	0.037	0.61	95	1.70	7.74	0.00	8.30	50.79	40.91
57-20/9 0–1	0.68	0.24	28.90	0.020	0.39	101	0.97	2.73	0.00	72.29	24.71	3.01
57-20/9 5–6	1.14	0.32	25.04	0.026	0.53	173	1.52	4.31	0.00	61.60	27.95	10.46
57-20/9 10–11	2.56	0.19	16.88	0.045	1.00	273	3.59	9.21	0.00	22.21	61.70	16.09
57-20/9 15–16	1.07	0.39	22.94	0.030	0.54	180	1.99	5.98	0.00	11.39	59.04	29.58
57-20/9 20–21	1.36	0.32	21.79	0.034	0.61	208	2.35	6.49	0.00	49.57	29.38	21.06
57-20/9 25–26	2.42	0.33	17.89	0.043	0.99	328	4.20	9.91	0.00	34.69	39.25	26.07
57-20/9 30–31	1.36	0.26	21.49	0.027	0.67	191	2.36	6.58	0.00	55.10	27.86	17.04
57-20/9 35–36	0.95	0.44	23.68	0.031	0.57	194	1.69	6.01	0.00	33.88	37.04	29.08
57-20/9 40–41	1.19	0.42	25.66	0.031	0.55	171	1.63	5.38	0.00	51.63	24.42	23.95
57-20/9 45–46	0.68	0.59	30.04	0.030	0.40	212	0.92	4.44	0.00	55.08	26.32	18.60
57-20/9 50–51	0.76	0.52	28.67	0.030	0.41	194	1.06	4.94	0.00	50.74	31.11	18.15
57-20/9 55–56	1.76	0.35	27.07	0.034	0.73	222	2.57	7.29	0.00	56.13	33.83	10.04
57-20/9 60–61	1.90	0.39	19.00	0.039	0.76	292	2.83	9.03	0.00	40.78	40.36	18.87
57-20/9 65–66	3.06	0.20	14.91	0.053	1.14	256	4.36	10.45	11.03	16.04	53.25	19.68
57-20/9 70–71	2.91	0.21	14.11	0.056	1.05	362	4.37	10.19	0.00	25.83	45.05	29.12
57-20/9 75–76	3.28	0.16	11.66	0.057	1.26	305	5.42	13.19	0.00	22.73	51.11	26.16
57-20/9 80–81	2.18	0.25	23.16	0.044	0.93	237	3.57	10.03	0.00	32.66	40.56	26.78
57-20/9 85–86	2.44	0.22	19.41	0.040	0.90	204	3.27	8.44	3.33	26.33	50.32	20.02
57-20/9 90–91	1.39	0.28	23.64	0.031	0.65	178	2.12	6.12	0.81	55.65	29.31	14.23

Table A1. *Cont.*

Samples	Fe (%)	Cd (ppm)	Ca (%)	P (%)	Mg (%)	Ba (ppm)	Al (%)	Total_REE (CC)	Gravel (%)	Sand (%)	Silt (%)	Clay (%)
57-20/9 95–96	2.14	0.21	18.47	0.036	0.85	233	3.31	8.34	0.00	35.39	49.54	15.07
57-20/9 100–101	1.37	0.31	20.40	0.030	0.66	243	2.46	6.50	0.00	58.57	32.47	8.96
57-20/9 105–106	0.90	0.52	25.74	0.031	0.54	193	1.32	5.27	0.00	45.20	35.76	19.03
57-20/9 110–111	0.82	0.63	26.82	0.034	0.53	280	1.38	4.96	0.00	37.74	39.37	22.89
57-20/9 115–116	0.78	0.58	27.20	0.027	0.51	245	1.22	4.81	0.00	62.90	27.08	10.02
57-20/9 120–121	1.54	0.49	25.94	0.034	0.68	285	2.62	7.63	0.00	62.64	25.41	11.96
57-20/9 125–126	1.59	0.32	26.27	0.036	0.74	293	2.55	7.03	0.00	63.01	26.60	10.40
57-20/9 130–131	2.42	0.38	17.21	0.049	1.00	396	4.57	10.43	0.00	34.13	38.69	27.19
57-20/9 133–134	1.72	0.34	18.29	0.041	0.96	385	3.87	8.83	5.86	20.22	49.67	24.25
57-20/9 135–136	2.04	0.15	15.33	0.045	1.71	402	4.38	8.86	0.00	11.65	50.04	38.32
57-20/9 140–141	2.63	0.11	9.01	0.048	1.52	479	5.42	10.39	0.00	3.55	58.01	38.45
57-20/9 145–146	2.52	0.18	17.58	0.039	0.96	289	3.83	10.87	7.26	45.74	37.74	9.27
57-20/9 150–151	3.71	0.11	10.82	0.054	1.38	345	5.84	13.45	0.00	20.10	55.14	24.76
57-20/9 155–156	2.68	0.22	17.46	0.044	1.09	283	4.34	11.89	0.00	36.64	38.76	24.60
57-20/9 160–161	1.26	0.31	27.98	0.029	0.70	181	2.02	6.22	0.00	60.84	23.88	15.28
57-20/9 165–166	1.27	0.38	25.48	0.027	0.62	307	2.60	6.05	10.77	21.61	42.73	24.90
57-20/9 170–171	1.05	0.29	22.27	0.027	0.46	335	2.59	5.59	0.00	41.97	37.30	20.74
57-20/9 175–176	1.30	0.38	25.57	0.029	0.59	261	2.35	6.47	0.00	53.88	26.79	19.33
57-20/9 180–181	0.79	0.50	29.33	0.031	0.39	222	1.23	4.80	0.00	42.86	31.98	25.16
57-20/9 185–186	2.53	0.22	16.76	0.041	0.94	757	4.30	9.68	0.00	35.15	51.86	12.99
57-20/9 190–191	1.47	0.35	27.05	0.035	0.68	255	2.48	7.48	0.00	50.63	29.52	19.85
57-20/9 195–196	1.22	0.46	29.32	0.031	0.54	183	1.87	5.49	2.13	43.37	23.03	31.47
57-20/9 200–201	1.29	0.38	28.26	0.029	0.56	203	2.12	6.29	0.00	46.47	40.71	12.82
57-20/10 0–1	0.85	0.24	31.27	0.023	0.45	130	1.18	3.51	0.00	68.56	25.96	5.48
57-20/10 5–6	1.28	0.23	28.77	0.030	0.53	161	1.60	5.07	0.00	62.59	29.18	8.23
57-20/10 10–11	2.19	0.21	21.70	0.039	0.88	265	3.26	9.45	7.14	50.19	34.36	8.30
57-20/10 15–16	2.98	0.16	15.37	0.050	1.17	349	4.60	11.32	0.00	43.14	43.79	13.07
57-20/10 20–21	1.94	0.36	19.60	0.048	0.89	288	3.75	8.89	0.00	29.85	42.29	27.86
57-20/10 25–26	1.61	0.31	20.97	0.038	0.75	274	3.11	8.15	0.00	26.94	43.07	29.99
57-20/10 30–31	1.95	0.24	18.51	0.040	0.89	290	3.71	8.93	0.00	20.16	52.63	27.21
57-20/10 35–36	1.67	0.33	22.08	0.041	0.78	254	3.18	8.48	0.00	36.18	41.78	22.04
57-20/10 40–41	1.50	0.39	25.39	0.044	0.74	200	2.87	9.10	0.75	26.85	40.43	31.98
57-20/10 45–46	1.75	0.30	23.58	0.050	0.73	199	2.49	8.08	0.00	37.12	37.78	25.11
57-20/10 50–51	0.82	0.59	30.01	0.037	0.51	194	1.50	5.88	0.00	46.17	30.41	23.42
57-20/10 55–56	0.94	0.34	27.19	0.033	0.50	200	1.81	6.08	0.67	48.47	28.30	22.56

Table A1. *Cont.*

Samples	Fe (%)	Cd (ppm)	Ca (%)	P (%)	Mg (%)	Ba (ppm)	Al (%)	Total_REE (CC)	Gravel (%)	Sand (%)	Silt (%)	Clay (%)
57-20/10 60–61	1.43	0.31	26.47	0.039	0.66	197	2.30	7.35	0.00	45.73	30.07	24.20
57-20/10 65–66	2.73	0.19	16.47	0.048	1.07	283	4.34	10.13	0.00	43.21	37.00	19.79
57-20/10 70–71	2.22	0.46	18.72	0.040	0.96	243	3.65	8.84	0.00	36.62	38.91	24.47
57-20/10 75–76	1.02	0.48	31.68	0.032	0.54	169	1.34	6.03	0.00	40.95	28.72	30.33
57-20/10 80–81	0.81	0.53	31.14	0.028	0.49	131	1.18	4.49	0.00	53.92	21.56	24.53
57-20/10 85–86	0.69	0.23	33.51	0.021	0.44	125	1.22	3.77	0.00	77.59	16.61	5.81
57-20/10 87–88	0.71	0.35	29.10	0.022	0.45	120	1.11	4.14	0.00	78.41	17.48	4.11
57-20/10 90–91	0.76	0.36	24.91	0.020	0.45	134	1.14	4.33	0.00	57.25	31.12	11.63
57-20/10 95–96	1.35	0.48	25.96	0.035	0.55	242	1.92	5.13	0.00	57.95	27.76	14.29
57-20/10 100–101	1.24	0.35	30.86	0.031	0.55	128	1.64	5.72	0.00	59.32	22.70	17.99
57-20/10 105–106	1.05	0.31	23.45	0.020	0.54	187	1.83	5.84	0.00	55.26	34.41	10.33
57-20/10 110–111	1.10	0.52	27.47	0.029	0.60	239	1.70	5.62	0.00	58.90	28.31	12.79
57-20/10 115–116	0.98	0.56	29.65	0.034	0.54	295	1.72	5.55	0.00	54.63	26.43	18.95
57-20/10 120–121	1.14	0.54	28.09	0.035	0.64	309	2.05	5.43	0.00	55.49	25.15	19.37
57-20/10 125–126	1.37	0.56	21.79	0.038	0.79	381	2.68	6.33	0.00	48.74	32.82	18.44
57-20/10 130–131	1.21	0.45	28.18	0.032	0.63	258	2.04	6.12	0.00	54.33	30.03	15.64
57-20/10 135–136	2.00	0.24	17.99	0.037	1.12	336	3.86	8.50	0.00	38.09	39.79	22.12
57-20/10 137–138	1.83	0.25	21.07	0.035	0.80	262	2.95	8.28	0.85	39.39	44.05	15.71
57-20/10 140–141	3.24	0.18	13.62	0.052	1.23	308	5.01	11.04	0.00	30.10	50.38	19.52
57-20/10 145–146	1.60	0.44	24.06	0.036	0.82	208	2.79	6.61	0.00	44.20	26.39	29.41
57-20/10 150–151	0.31	1.12	37.05	0.040	0.47	138	0.49	3.55	0.00	5.05	35.37	59.59
57-20/10 152–153	0.21	1.13	37.88	0.040	0.44	80	0.40	3.26	0.00	7.14	29.88	62.99
57-20/10 155–156	1.28	0.73	34.56	0.040	0.68	134	1.26	5.02	0.00	29.90	39.05	31.05
57-20/10 160–161	0.80	0.51	33.18	0.028	0.49	189	1.14	3.53	0.00	47.39	26.25	26.37
57-20/10 165–166	0.91	0.43	31.61	0.026	0.51	555	1.40	4.65	0.00	60.27	19.89	19.84
57-20/10 170–171	0.87	0.41	31.79	0.025	0.51	146	1.30	4.05	0.00	61.80	25.89	12.31
57-20/10 175–176	0.94	0.40	33.20	0.025	0.50	210	1.44	4.57	0.00	58.75	21.80	19.46
57-20/10 180–181	2.67	0.23	16.75	0.046	1.01	395	4.34	8.90	1.56	54.76	31.94	11.74
57-20/10 185–186	2.45	0.24	19.87	0.038	0.94	277	3.95	10.21	0.00	36.95	43.21	19.85
57-20/10 190–191	1.44	0.31	26.63	0.029	0.60	167	2.17	7.88	0.00	49.36	36.18	14.46
57-20/10 195–196	1.26	0.27	25.92	0.029	0.58	196	2.08	6.66	0.00	61.65	29.11	9.25
57-20/11 0–1	0.61	0.17	20.49	0.016	0.34	123	1.00	2.34	0.00	81.84	15.52	2.64
57-20/11 5–6	2.57	0.28	22.03	0.049	1.03	198	2.63	7.90	0.00	61.43	27.09	11.47
57-20/11 10–11	3.05	0.17	15.01	0.048	1.14	340	4.55	10.48	0.89	41.84	44.21	13.06
57-20/11 15–16	1.57	0.39	21.07	0.038	0.77	244	2.97	7.97	23.08	26.48	27.58	22.86

Table A1. *Cont.*

Samples	Fe (%)	Cd (ppm)	Ca (%)	P (%)	Mg (%)	Ba (ppm)	Al (%)	Total_REE (CC)	Gravel (%)	Sand (%)	Silt (%)	Clay (%)
57-20/11 20–21	1.83	0.30	20.28	0.040	0.84	271	3.36	8.30	0.00	35.51	40.44	24.06
57-20/11 25–26	1.76	0.43	25.33	0.043	0.79	204	3.11	8.49	0.90	29.90	37.93	31.27
57-20/11 30–31	2.11	0.27	19.54	0.041	0.93	250	3.85	8.98	0.00	32.34	43.38	24.28
57-20/11 35–36	0.91	0.32	26.95	0.026	0.55	156	1.58	5.30	0.00	63.27	20.62	16.12
57-20/11 40–41	1.66	0.43	23.76	0.040	0.75	236	2.96	8.81	0.00	34.58	35.49	29.94
57-20/11 45–46	1.77	0.38	22.05	0.040	0.86	242	3.35	8.79	0.00	20.31	42.09	37.60
57-20/11 50–51	0.68	0.41	30.32	0.026	0.48	143	1.06	4.29	0.00	36.09	34.77	29.14
57-20/11 55–56	0.60	0.79	32.86	0.043	0.44	140	1.05	5.57	0.00	2.93	36.75	60.33
57-20/11 60–61	1.76	0.48	30.10	0.054	0.75	150	1.93	6.62	10.00	40.13	22.62	27.25
57-20/11 65–66	1.08	0.41	31.67	0.037	0.63	150	1.56	6.24	0.00	60.81	22.71	16.48
57-20/11 70–71	0.95	0.48	32.62	0.035	0.54	137	1.38	5.72	0.00	49.96	23.33	26.72
57-20/11 75–76	0.42	0.27	33.29	0.014	0.36	74	0.71	3.03	0.00	82.32	13.38	4.30
57-20/11 80–81	0.77	0.50	31.03	0.023	0.48	145	1.24	4.55	0.00	75.08	16.27	8.65
57-20/11 85–86	1.45	0.34	29.77	0.029	0.61	182	2.21	7.76	0.00	60.46	28.84	10.70
57-20/11 90–91	1.04	0.23	30.09	0.024	0.54	153	1.66	6.12	0.00	77.01	19.59	3.40
57-20/11 95–96	1.51	0.42	25.20	0.033	0.70	283	2.65	7.55	0.00	56.33	23.79	19.88
57-20/11 100–101	1.06	0.64	30.62	0.032	0.61	280	1.71	6.44	0.00	53.47	24.45	22.08
57-20/11 105–106	3.26	0.20	14.51	0.049	1.21	306	4.96	12.88	12.41	28.63	36.44	22.53
57-20/11 110–111	1.13	0.49	29.54	0.033	0.67	163	2.08	6.47	0.00	37.63	30.95	31.42
57-20/11 115–116	0.31	0.63	35.94	0.030	0.41	79	0.51	3.28	0.00	32.60	29.52	37.88
57-20/11 120–121	0.36	0.80	36.15	0.032	0.41	70	0.61	3.43	0.00	16.72	27.07	56.21
57-20/11 125–126	0.67	0.55	35.83	0.028	0.45	126	0.89	3.79	0.00	58.79	16.36	24.85
57-20/11 130–131	0.90	0.28	29.09	0.023	0.50	111	1.30	4.67	0.00	72.98	19.31	7.71
57-20/11 135–136	1.29	0.39	28.28	0.028	0.54	191	1.86	6.17	0.00	60.37	22.12	17.51
57-20/11 140–141	2.24	0.23	19.86	0.036	0.81	366	3.76	9.26	0.00	55.32	32.00	12.68
57-20/11 145–146	2.43	0.21	20.56	0.043	0.92	266	3.92	10.63	0.00	45.66	37.64	16.71

References

1. MacLachlan, S.E.; Elliot, G.M.; Parson, L.M. Investigations of the bottom current sculpted margin of Hatton bank, NE Atlantic. *Mar Geol.* **2008**, *253*, 170–184. [CrossRef]
2. Hitchen, K. The geology of the UK Hatton–Rockall margin. *Mar. Pet. Geol.* **2004**, *21*, 993–1012. [CrossRef]
3. Stow, D.A.V.; Lovell, J.P.B. Contourites: Their recognition in modern and ancient sediments. *Earth Sci. Rev.* **1979**, *14*, 251–291. [CrossRef]
4. Stow, D.; Holbrook, J.A. Hatton Drift contourites, Northeast Atlantic, Deep Sea Drilling Project LEG 81. In *Initial Reports DSDP*; Roberts, D.G., Schnitker, D., Eds.; ODP Proceedings Series; American Geoscience Instiute: Washington, DC, USA, 1983; Volume 81.
5. Ruddiman, W.F. Sediment redistribution on the Reykjanes Ridge: Seismic evidence. *Geol. Soc. Am. Bull.* **1972**, *82*, 2039–2062. [CrossRef]
6. McCave, I.N.; Tucholke, B.E. Deep–current controlled sedimentation in the Western North Atlantic. In *The geology of North America, The Western North Atlantic Region, Decade of North American Geology*; Vogt, P.R., Tucholke, B.E., Eds.; Geological Society of America: Boulder, CO, USA, 1986; Volume M, pp. 451–467.
7. Faugères, J.C.; Mézerais, M.L.; Stow, D.A.V. Contourite drift types and their distribution in the North and South Atlantic Ocean Basins. *Sed Geol.* **1993**, *82*, 189–203. [CrossRef]
8. Faugères, J.C.; Stow, D.A.V.; Imbert, P.; Viana, A.R. Seismic features diagnostic of contourite drifts. *Mar Geol.* **1999**, *162*, 1–38. [CrossRef]
9. McCave, I.N.; Lonsdale, P.F.; Hollister, C.D.; Gardner, W.D. Sediment transport over the Hatton and Gardar contourite drifts. *J. Sed. Petrol.* **1980**, *50*, 1049–1062.
10. Bianchi, G.G.; McCave, I.N. Hydrography and sedimentation under the deep western boundary current on Björn and Gardar Drifts, Iceland Basin. *Mar Geol.* **2000**, *165*, 137–169. [CrossRef]
11. Huizhong, W.; McCave, I.N. Distinguishing climatic and current effects in mid–Pleistocene sediments of Hatton and Gardar Drifts, NE Atlantic. *J. Geol. Soc. Lond.* **1990**, *147*, 373–383. [CrossRef]
12. Weaver, P.P.E.; Wynn, R.B.; Kenyon, N.H.; Evans, J. Continental margin sedimentation, with special reference to the north–east Atlantic margin. *Sedimentology* **2000**, *47*, 239–256. [CrossRef]
13. Stow, D.A.V.; Holbrook, J.A. Hatton Drift contourites, northeast Atlantic, deep sea drilling project LEG 81. *Univ. Edinb.* **1984**, *25*, 695–699.
14. Hopkins, T.S. *The GIN Sea SACLANTCEN*; Report SR–124; Saclant Undersea Research Centre: La Spezia, Italy, 1988; pp. 1–190.
15. Van Aken, H.M. Mean currents and current variability in the Iceland Basin. *J. Sea Res.* **1995**, *33*, 135–145. [CrossRef]
16. Van Aken, H.M. The hydrography of the mid–latitude northeast Atlantic Ocean I: The deep water masses. *Deep Sea Res. I* **2000**, *47*, 757–788. [CrossRef]
17. Yashayaev, I.; Clarke, A. Evolution of North Atlantic water masses inferred from Labrador Sea salinity series. *Oceanography* **2008**, *21*, 30–45. [CrossRef]
18. Yashayaev, I.; Dickson, B. Transformation and Fate of the Overflows in the Northern North Atlantic. In *Artic–Subartic Ocean Fluxes*; Dickson, R.R., Meincke, J., Rhines, P., Eds.; Springer: Berlin, Germany, 2008; pp. 505–536.
19. Maslin, M.A.; Shackleton, N.J.; Pflaumann, U. Surface water temperature, salinity and density changes in the northeast Atlantic during the last 45,000 years: Heinrich events, deep water formation and climatic rebounds. *Paleoceanography* **1995**, *10*, 527–544. [CrossRef]
20. Robinson, S.G.; Maslin, M.A.; McCave, N. Magnetic susceptibility variations in upper Pleistocene deep–sea sediments of the NE Atlantic: Implications for ice rafting and paleocirculation at the Last Glacial Maximum. *Paleoceanography* **1995**, *10*, 221–250. [CrossRef]
21. Barker, S.; Kiefer, T.; Elderfield, H. Temporal changes in North Atlantic circulation constrained by planktonic foraminiferal shell weights. *Paleoceanography* **2004**, *19*, 1–15. [CrossRef]
22. Amante, C.; Eakins, B.W. *ETOPO1 Global Relief Model: Procedures, Data Sources and Analysis*; NOAA Tech. Memo. NESDIS NGDC–24; NOAA: Silver Spring, MD, USA, 2009; p. 19. [CrossRef]
23. Kissel, C.C.; Laj, L.; Labeyrie, T.; Dokken, A.; Voelker, D. Blamart. Rapid climatic variations during marine isotopic stage 3: Magnetic analysis of sediments from Nordic Seas and North Atlantic. *Earth Planet. Sci. Lett.* **1999**, *171*, 489–502. [CrossRef]

24. Alley, R.B.; Clark, P.U. The deglaciation of the northern hemisphere: A global perspective. *Annu. Rev. Earth Planet. Sci. Lett.* **1999**, *27*, 149–182. [CrossRef]
25. Chi, J.; Mienert, J. Linking physical property records of Quaternary sediments to Heinrich events. *Mar. Geol.* **1996**, *131*, 57–73. [CrossRef]
26. Heinrich, H. Origin and consequences of cyclic ice–rafting in the Northeast Atlantic Ocean during the past 130,000 years. *Quat. Res.* **1988**, *29*, 142–152. [CrossRef]
27. Bond, G.C.; Lotti, R. Iceberg discharges into the North Atlantic on millennial time Scales during the Last Glaciation. *Science* **1995**, *267*, 1005–1009. [CrossRef] [PubMed]
28. Andrews, J.T. Icebergs and iceberg rafted detritus (IRD) in the North Atlantic: Facts and assumptions. *Oceanography* **2000**, *13*, 100–108. [CrossRef]
29. Kissel, C. Magnetic signature of rapid climatic variations in glacial North Atlantic, a review. *C. R. Geosci.* **2005**, *337*, 908–918. [CrossRef]
30. Hemming, S.R. Heinrich events: Massive late Pleistocene detritus layers of the North Atlantic and their global climate imprint. *Rev. Geophys.* **2004**, *42*, RG1005. [CrossRef]
31. Stanford, J.D.; Rohling, E.J.; Bacon, S.; Roberts, A.P.; Grousset, F.E.; Bolshaw, M. A new concept for the paleoceanographic evolution of Heinrich event 1 in the North Atlantic. *Quat. Sci. Rev.* **2011**, *30*, 1047–1066. [CrossRef]
32. Bond, G.C.; Broecker, W.S.; Johnsen, S.; McManus, J.F.; Labeyrie, L.; Jouzel, J.; Bonani, G. Correlation between climate records from North Atlantic sediments and Greenland ice. *Nature* **1993**, *365*, 143–147. [CrossRef]
33. Broecker, W.S. Massive iceberg discharges as triggers for global climate change. *Nature* **1994**, *372*, 421–424. [CrossRef]
34. Broecker, W.S.; Bond, G.; McManus, J.; Klas, M.; Clark, E. Origin of the Northern Atlantic's Heinrich events. *Clim. Dyn.* **1992**, *6*, 265–273. [CrossRef]
35. Ruddiman, W.F. Late Quaternary deposition of ice-rafted sand in the subpolar North Atlantic (lat 40° to 65°). *Geol. Soc. Am. Bull.* **1977**, *88*, 1813–1827. [CrossRef]
36. Bond, G.C.; Heinrich, H.; Broecker, W.S.; Labeyrie, L.; McManus, J.; Andrews, J.; Huon, S.; Jantschik, R.; Clasen, S.; Simet, C.; et al. Evidence for massive discharges of icebergs into the North Atlantic Ocean during the last glacial period. *Nature* **1992**, *360*, 245–249. [CrossRef]
37. Thomson, J.; Higgs, N.C.; Clayton, T. A geochemical criterion for the recognition of Heinrich events and estimation of their depositional fluxes by the 230Thexcess profiling method. *Earth Planet. Sci. Lett.* **1995**, *135*, 41–56. [CrossRef]
38. McManus, J.F.; Anderson, R.F.; Broecker, W.S.; Fleisher, M.Q.; Higgins, S.M. Radiometrically determined sedimentary fluxes in the sub–polar North Atlantic during the last 140,000 years. *Earth Planet. Sci. Lett.* **1998**, *155*, 29–43. [CrossRef]
39. Bard, E.; Rostek, F.; Turon, J.-L.; Gendreau, S. Hydrological impact of Heinrich events in the subtropical northeast Atlantic. *Science* **2000**, *289*, 1321–1324. [CrossRef] [PubMed]
40. Stoner, J.S.; Channell, J.E.T.; Hillaire-Marcel, C. The magnetic signature of rapidly deposited detrital layers from the deep Labrador Sea: Relationship to North Atlantic Heinrich layers. *Paleoceanography* **1996**, *11*, 309–325. [CrossRef]
41. Walden, J.; Wadsworth, E.; Austin, W.E.N.; Peters, C.; Scourse, J.D.; Hall, I.R. Compositional variability of ice-rafted debris in Heinrich layers 1 and 2 on the northwest European continental slope identified by environmental magnetic analyses. *J. Quat. Sci.* **2007**, *22*, 163–172. [CrossRef]
42. Grousset, F.E.; Cortijo, E.; Huon, S.; Hervé, L.; Richter, T.; Burdloff, D.; Duprat, J.; Weber, O. Zooming in on Heinrich layers. *Paleoceanography* **2001**, *16*, 240–259. [CrossRef]
43. Manighetti, B.; McCave, J.N. Depositional fluxes, palaeoproductivity, and ice rafting in the NE Atlantic over the past 30 ka. *Paleoceanography* **1995**, *10*, 579–592. [CrossRef]
44. Hinrichs, J.; Schnetger, B.; Schale, H.; Brumsack, H.J. A High resolution study of NE Atlantic sediments at station Bengal: Geochemistry and early diagenesis of Heinrich layers. *Mar. Geol.* **2001**, *177*, 79–92. [CrossRef]
45. Cortijo, E.; Labeyrie, L.; Vidal, L.; Vautravers, M.; Chapman, M.; Duplessy, J.-C.; Elliot, M.; Arnold, M.; Turon, J.-L.; Auffret, G. Changes in sea surface hydrology associated with Heinrich event 4 in the North Atlantic Ocean between 40_ and 60_N. *Earth Planet. Sci. Lett.* **1997**, *146*, 29–45. [CrossRef]

46. Vidal, L.; Labeyrie, L.; Cortijo, E.; Arnold, M.; Duplessy, J.C.; Michel, E.; Becque, S.; van Weering, T.C.E. Evidence for changes in the North Atlantic Deep Water linked to meltwater surges during the Heinrich events. *Earth Planet. Sci. Lett.* **1997**, *146*, 13–27. [CrossRef]
47. Elliot, M.; Labeyrie, L.; Duplessy, J.C. Changes in North Atlantic deep–water formation associated with the Dansgaard–Oeschger temperature oscillations (60–10 ka). *Quat. Sci. Rev.* **2002**, *21*, 1153–1165. [CrossRef]
48. Paillard, D.; Labeyrie, L. Role of the thermohaline circulation in the abrupt warming after Heinrich events. *Nature* **1994**, *372*, 162–164. [CrossRef]
49. Manighetti, B.; McCave, I.N.; Maslin, M.; Shackleton, N.J. Chronology for climate change: Developing age models for the Biogeochemical Ocean Flux Study cores. *Paleoceanography* **1995**, *10*, 513–525. [CrossRef]
50. Jennerjahn, T.C.; Ittekkot, V.; Arz, H.W.; Behling, H.; Pätzold, J.; Wefer, G. Asynchronous Terrestrial and Marine Signals of Climate Change During Heinrich Events. *Science* **2004**, *306*, 2236–2239. [CrossRef]
51. Folk, R.L. The distinction between grain size and mineral composition in sedimentary rock nomenclature. *J. Geol.* **1954**, *62*, 344–359. [CrossRef]
52. Folk, R.L.; Ward, W.C. Brazos River bar: A study in the significance of grain size parameters. *J. Sedim. Petrol.* **1957**, *27*, 3–26. [CrossRef]
53. Wedepohl, H. The composition of the continental crust. *Geochim. Cosmochim. Acta* **1995**, *59*, 1217–1239. [CrossRef]
54. Wilkinson, I. *Microfaunal Analyses of Two Cores from Hatton Bank, North Atlantic*; Internal Report IR/09/088; British Geological Survey: Nottingham, UK, 2010.
55. Robinson, S.G.; McCave, I.N. Orbital forcing of bottom–current enhanced sedimentation on Feni Drift, NE Atlantic, during the mid–Pleistocene. *Paleoceanography* **1994**, *9*, 943–972. [CrossRef]
56. Lebreiro, S.M.; Voelker, A.H.L.; Vizcaino, A.; Abrantes, F.G.; Alt–Epping, U.; Jung, S.; Thouveny, N.; Gràcia, E. Sediment instability on the Portuguese continental margin under abrupt glacial climate changes (last 60 kyr). *Quat. Sci. Rev.* **2009**, *28*, 3211–3223. [CrossRef]
57. Andrews, J.T. Abrupt changes (Heinrich events) in late Quaternary North Atlantic marine envrionments: A history and review of data and concepts. *J. Quat. Sci.* **1998**, *13*, 3–16. [CrossRef]
58. Peters, C.; Austin, W.E.N.; Walden, J.; Hibbert, F.D. Magnetic characterisation and correlation of a Younger Dryas tephra in North Atlantic marine sediments. *J. Quat. Sci.* **2010**, *25*, 339–347. [CrossRef]
59. Olfield, F.; Appleby, P.G.; Thompson, R. Palaeoecological studies of lakes in the highlands of Papua New Guinea. *J. Ecol.* **1980**, *68*, 457–477. [CrossRef]
60. Van de Bogaard, C.; Dörfler, W.; Sandgren, P.; Schmincke, H.U. Correlating the Holocene records: Icelandic tephra found in Schleswig–Holstein (northern Germany). *Naturwissenschaften* **1994**, *81*, 554–556. [CrossRef]
61. Andrews, J.T.; Geirsdóttir, A.; Hardardóttir, J.; Principato, S.; Grönvold, K.; Kristjansdóttir, G.B.; Helgadóttir, G.; Drexler, J.; Sveinbjörnsdóttir, A. Distribution, sediment magnetism and geochemistry of the Saksunarvatn (10 180 ± 60 cal. yr BP) tephra in marine, lake and terrestrial sediments, northwest Iceland. *J. Quat. Sci.* **2002**, *17*, 731–745. [CrossRef]
62. Andrews, J.T.; Hardardóttir, J.; Stoner, J.S.; Mann, M.E.; Kristjansdóttir, G.B.; Koc, N. Decadal to millennial–scale periodicities in North Icealnd shelf sedimetns over the last 12000 cal yr: Long–term North Atlantic oceanographic variability and solar forcing. *Earth Planet. Sci. Lett.* **2003**, *210*, 453–465. [CrossRef]
63. Lacasse, C.; Sigurdsson, H.; Carey, S.; Paterne, M.; Guichard, F. North Atlantic deep–sea sedimentation of Late Quaternary tephra from the Iceland hotspot Source. *Mar. Geol.* **1996**, *129*, 207–235. [CrossRef]
64. Bard, E.; Arnold, M.; Mangerud, J.; Paterne, M.; Labeyrie, L.; Duprat, J.; Mélières, M.-A.; Sønstegaard, E.; Duplessy, J.C. The North Atlantic atmosphere–sea surface 14 C gradient during the Ypunger Dryas climatic event. *Earth Planet. Sci. Lett.* **1994**, *126*, 275–287. [CrossRef]
65. Lane, C.S.; Blockley, S.P.E.; Mangerud, J.; Smith, V.C.; Lohne, Ø.S.; Tomlinson, E.L.; Matthews, I.P.; Lotter, A.F. Was the 12.0 ka Icelandic Vedde Ash one of a kind? *Quat. Sci. Rev.* **2012**, *33*, 87–99. [CrossRef]
66. Arz, H.W.; Patzold, J.; Wefer, G. The deglacial history of the western tropical Atlantic as inferred from high resolution stable isotope records off northeastern Brazil. *Earth Planet. Sci. Lett.* **1999**, *167*, 105–117. [CrossRef]
67. Adegbie, A.T.; Schneider, R.R.; Röhl, U.; Wefer, G. Glacial millennial–scale fluctuations in central African precipitation recorded in terrigenous sediment supply and freshwater signals offshore Cameroon. *Palaeogeogr. Palaeoclimatol. Palaeoecol.* **2003**, *197*, 323–333. [CrossRef]

68. Heil, G.M.N.; Arz, H.W.; Behling, H.; Wefer, G. Extent of high northern latitude forcing on tropical/subtropical South American precipitation during the last glacial. *Geophys. Res. Abstr.* **2006**, *8*, 07138.
69. Revel, M.; Cremer, M.; Grousset, F.E.; Labeyrie, L. Grain-size and Sr–Nd isotopes as tracer of paleo-bottom current strengh, Northeast Atlantic Ocean. *Mar. Geol.* **1996**, *131*, 233–249. [CrossRef]
70. Watkind, S.J.; Maher, B.A. Magnetic characterization of present-day deep-sea sediments and sources in the North Atlantic. *Earth Planet. Sci. Lett.* **2003**, *214*, 379–394. [CrossRef]
71. Pirrung, M.; Fütterer, D.; Grobe, H.; Matthiessen, J.; Niessen, F. Magnetic susceptibility and ice-rafted debris in surface sedimens of the Nordic Seas: Implications for Isotope Stage 3 oscillations. *Rev. Geophys.* **2002**, *22*, 1–11.
72. Peck, V.L.; Hall, I.R.; Zahn, R.; Grousset, F.; Hemming, S.R.; Scourse, J.D. The relationship of Heinrich events and their European precursors over the past 60 ka BP: A multi-proxy ice-rafted debris provenance study in the North Atlantic. *Quat. Sci. Rev.* **2007**, *26*, 862–875. [CrossRef]
73. Bond, G.C.; Showers, W.; Elliot, M.; Evans, M.; Lotti, R.; Hajdas, I.; Bonani, G.; Johnsen, S. The North Atlantic's 1–2 kyr climate rhythm: Relation to Heinrich events, Dansgaard/Oeschger cycles and the little ice age. In *Mechanisms of Global Climate Change at Millennial Time Scales*; Geophysical Monograph Series; Clark, P.U., Webb, R.S., Keigwin, L.D., Eds.; AGU: Washington, DC, USA, 1999; Volume 112, pp. 35–68.
74. Hemming, S.R.; Hall, C.M.; Biscaye, P.E.; Higgins, S.M.; Bond, G.C.; McManus, J.F.; Barber, D.C.; Andrews, J.T.; Broecker, W.S. 40Ar/39Ar ages and 40Ar* concentrations of fine–grained sediment fractions from North Atlantic Heinrich layers. *Chem. Geol.* **2002**, *182*, 583–603. [CrossRef]
75. Grousset, F.E.; Pujol, C.; Labeyrie, L.; Auffret, G.; Boelaert, A. Were the North Atlantic Heinrich events triggered by the behavior of the European ice sheets? *Geology* **2000**, *28*, 123–126. [CrossRef]
76. Rasmussen, T.L.; Thomsen, E. The role of the North Atlantic Drift in the millennial timescale glacial climate fluctuations. *Palaeogeogr. Palaeoclimatol. Palaeoecol.* **2004**, *210*, 101–116. [CrossRef]
77. Calvert, S.E.; Pedersen, T.F. Elemental proxies for Palaeoclimatic and Palaeoceanographic Variability in Marine Sediments: Interpretation and Application. In *Proxies in Late Cenozoic Paleoceanography*; Hillarie–Marcel, C., De Vernal, A., Eds.; Elsevier: Amsterdam, The Netherlands, 2007; pp. 567–644.
78. Bertram, C.J.; Elderfield, H.; Shackleton, N.J.; Mac–Donald, J.A. Cadmium/calcium and carbon isotope reconstructions of the glacial northeast Atlantic Ocean. *Paleoceanography* **1995**, *10*, 563–578. [CrossRef]
79. Gwiazda, R.H.; Hemming, S.R.; Broecker, W.S. Provenance of icebergs during Heinrich event 3 and the contrast to their sources during other Heinrich episodes. *Paleoceanography* **1996**, *11*, 371–378. [CrossRef]